Bioprocess and Biosystems Engineering (2022) 45:1825–1837
https://doi.org/10.1007/s00449-022-02789-7

RESEARCH PAPER

Bio-approach: preparation of RGO-AgNPs on cotton fabric and interface with sweat environment for antibacterial activity

Perumal Dhandapani[1] · Murali Santhoshkumar[2] · Jayaraman Narenkumar[3] · Mohamad S. AlSalhi[4] · Paulraj Arun Kumar[5] · Sandhanasamy Devanesan[4] · Seenivasan Kokilaramani[1] · Aruliah Rajasekar[1]

Received: 21 June 2022 / Accepted: 8 September 2022 / Published online: 25 September 2022
© The Author(s), under exclusive licence to Springer-Verlag GmbH Germany, part of Springer Nature 2022

Abstract

This study aims to develop a reduced graphene oxide (RGO)-silver nanoparticles (AgNPs) coating on the cotton fabric (CT) surface using photoreduction with a hydrothermal process and evaluate the antibacterial activity in a sweat environment. An ureolytic bacterium of *Bacillus subtilis* (HM475276) was used to generate ammonia from synthetic urine. RGO-AgNPs were synthesized on the CT surface using a moderate dosage of 1% silver ammonium complex. The analytical study reveals that spherical-shaped AgNPs of 10–50 nm size were uniformly anchored throughout the RGO sheet on the CT, further supported by X-ray photoelectron spectroscopic analysis (XPS). X-ray powder diffraction (XRD) and Energy-dispersive X-ray absorption spectroscopy (EDAX) elemental mapping confirmed Ag/AgCl formation on CT treated with sweat. The sustained release of Ag^+ ions from the treated CT in the sweat solution was assessed by atomic absorption spectroscopy (AAS) and ranged from 2 to 8 ppm, correlated with antibacterial activity. The agar diffusion and solution suspension method to demonstrate the combat bacterial species were greater on RGO-AgNPs-CT than sweat-treated CT due to the suppression of Ag^+ ion release caused by the deposition of Ag/AgCl. Hence, sweat-treated RGO-AgNPs-CT proved to have higher inactivation activity (45 min) than sweat-treated AgNPs-CT (60 min) due to the RGO-Ag/AgCl serving photocatalyst influencing hydroxyl radical (OH^-) formation under sunlight. The RGO-AgNPs-CT has confirmed that it retains antibacterial activity after passing the laundry durability test. Together, the results showed an opportunity for improved functional fabrics that are exceptional at combating bacterial pathogens and holding up well to laundry durability tests.

Keywords Biological activated ammonia · Reduced graphene oxide · AgNPs · Cotton fabric · Antibacterial activity

Introduction

The cotton fabric (CT) has been primarily used in the medical environment for wound dressing and controlling bacterial infection from vulnerable atmospheric conditions [1]. The polymeric cellulose structure of CT renders excellent moisture adsorption and O_2 distribution properties due to free space between the fiber cloth, which allows air to circulate and move freely through the material [2]. Cotton materials are primarily in contact with the skin's surface to absorb sweat and body temperature [2]. These features allow bacteria to adhere to the CT surface, developing a biofilm that causes unpleasant odours, stain removal, fabric deterioration, and even physical discomfort such as skin allergies and disease [2]. As a result, manufacturing antibacterial cotton fabric is considered in medical textile finishing and a clever way to restrict the spread of bacterial infection after a wound healing treatment. The antibacterial behaviour of the fabric

✉ Sandhanasamy Devanesan
sdnesan1981@gmail.com

✉ Aruliah Rajasekar
rajasekargood@gmail.com

1 Environmental Molecular Microbiology Research Laboratory, Department of Biotechnology, Thiruvalluvar University, Serkkadu, Vellore, Tamilnadu 632115, India

2 Department of Biotechnology, Thiruvalluvar University, Serkkadu, Vellore, Tamilnadu 632115, India

3 Centre for Materials Engineering and Regenerative Medicine, Bharath Institute of Higher Education and Research, Selaiyur, Chennai, Tamil Nadu 600073, India

4 Department of Physics and Astronomy, College of Science, King Saud University, P.O. Box. 2455, Riyadh 11451, Saudi Arabia

5 School of Chemical Engineering, Chonnam National University, Gwangju, South Korea

surface was prepared by including various nanomaterials such as Ag, Cu/CuO, TiO_2, and ZnO [3–5]. Many efforts have been made to investigate the application of AgNPs to different textile materials [6–8]. Recent advances in the ideal synthesis of AgNPs were made on the fabric surface from silver ammonium complex using the mild-hydrothermal method [9–11]. Aside from these methods, biological activated ammonia was produced from synthetic urine using ureolytic bacterium and synthesized AgNPs on the hydroxyapatite particle surface to prevent bacterial attachment and proliferation as described in previous studies [12]. Several investigators have focused on biologically synthesized AgNPs nanoparticles due to the cost-effective and eco-friendly approach [13, 14]. Biological processes synthesized various morphology of AgNPs by using plant extracts, fungi, and bacterial species and then decorated the fabric surface to improve antibacterial activity [14].

The cumulative release of Ag^+ ion from AgNPs-coated CT and its interaction with the bacterial cell membrane by electrostatic forces leads to cell death [15, 16]. Various mechanisms for the mode of action of AgNPs involved in the antibacterial activity of several bacterial species have been proposed [17, 18]. The influence of varied physicochemical features of AgNPs on their interaction with chloride, sulphate, and phosphate ions in biological media was apparent as the subsequent change of dissolution level of Ag^+ ions from AgNPs surface predicate the antibacterial activity pathways [19, 20]. The existing reports only address the stability of AgNPs on CT in sweat solution, which is relevant to the antibacterial activity investigated [21–23]. Changes in the crystal phase and morphology of AgNPs on the fabric surface triggered by Cl^- ion from sweat solution in a wet environment and their antimicrobial action have not been explored. Our preliminary work synthesized AgNPs on fabric by adopting organic polymers as functional group intermediates, facilitating Ag^+ ion release towards antibacterial activity [8]. For instance, achieving the rapid adherence of AgNPs to fabric surfaces has proven to be challenging for the progress of textile finishing. The graphene sheet is an appropriate support material for nanoparticle (NPs) loading; AgNPs placed onto the graphene sheet decreased particle aggregation, facilitated nanomaterial stability, combated pathogens, and hindered bacterial cell adhesion [24–27]. The graphene-coated fabric has been investigated for various biomedical applications, including antibacterial activity, dressing, hydrogel, coating on an electronic device for health monitoring, and protection against bacterial infections and viruses [24–27].

In the present study, we demonstrated a facile bio-approach combined with photoreduction and a hydrothermal synthesis of AgNPs on the RGO sheet at the interface of the CT to investigate antibacterial activity with and without a sweat environment. The Cl^- ions absorption on the treated CT in sweat solution and silver chloride (AgCl) formation were analyzed by UV–visible spectroscopy, XRD, EDAX elemental mapping, Field emission-scanning electron microscopy (FE-SEM), and Transmission electron microscopy (TEM). AAS was used to explore the cumulative Ag^+ ion release from sweat-treated and untreated CT, and influences on antibacterial activity were elucidated. Moreover, a comparison study on the antibacterial activity of sweat-treated and untreated fabric samples against *Escherichia coli* (*E. coli*), *Staphylococcus aureus* (*S. aureus*), and *Bacillus subtilis* 5B (*B. subtilis* 5B) was conducted. In addition, the photoinactivation performance of the sweat-treated RGO-AgNPs-CT against *E.coli* bacterium was performed, and its correlation with sunlight intensity has been discussed.

Materials and methods

Preparation of RGO-AgNPs wrap on the fabric surface

The modified Hummers method [28] generated graphene oxide sheets (GO) from graphite flakes. For the present study, cotton fabric (woven) was used, and it was 100% cotton with natural colour. The supporting information describes the preparation of biologically activated ammonia from synthetic urine using *B. subtilis* (HM475276), enrichment of bacterial culture, pH measurement, and estimation of ammonium content (S1). In this study, 10 ml of GO solution (2 mg/ml) was mixed with 90 ml of Milli-Q and ultrasonically dispersed for 2 h. The CT sample was pieced into 5.0×10.0 cm^2 after cleaning. The CT sample was immersed in GO solution for 60 min while being gently shaken at 50 rpm. The finished fabric is known as a GO-coated fabric sample (GO-CT). The 1% silver ammonium complex was made up of biologically activated ammonia and $AgNO_3$. For 15 min, the GO-CT sample was immersed in a 1% silver ammonium complex solution. Following that, the photoreactor medium (GO and silver ammonium complex) with CT samples were exposed to light irradiation for 10 min using solar simulators (Class AAA solar simulator Science tech—Canada) at maximum light intensity (1,00,000 Lux). The photo-treated cotton fabric samples were forceps-up collected from the medium and rinsed with Milli-Q water to remove the residues. Afterwards, the fabric was poured into a Teflon-lined stainless steel autoclave and heated for 1 h at 80 °C and 8 h at 120 °C. The fabric samples were dried overnight in a vacuum oven at 60 °C. A similar method was used to develop RGO-AgNPs without fabric.

Characterization of RGO-AgNPs coated with fabric

The crystal phase analysis of the tested fabric sample was performed using an XRD, the D8-ADVANCE PXRD (BRUKER). The surface morphology of the bare and treated CT samples was studied using FE-SEM with a Carl Zeiss SUPRA 55 VP. The weight loss of plain and treated CT by TA Instruments SDT Q600 from room temperature to 800 °C at a heating rate of 5 °C/min in the presence of air. A Varian spectrophotometer was used to record the UV–visible absorption spectra of both cotton fabrics (before and after treated samples) at 200–800 nm.

Treatment of sweat in RGO-AgNPs coated with fabric

Sweat solution was made according to ISO 3160-2 standards (20 g/L NaCl, 17.5 g/L NH_4OH, 5 g/L acetic acid, and 15 g/L lactic acid) [22]. CT samples, both treated and untreated, were kept moist for 30 min by adding 2 ml of sweat solution drop by drop to the fabric surface. The CT samples were gently air-dried after sweat treatment. Sweat-bare-CT, sweat-GO-CT, sweat-AgNPs-CT, and sweat-RGO-AgNPs-CT samples were noted. The CT samples regarding interface changes in the Cl^- ion adsorption from sweat solution by employing EDAX (Bruker).

In addition, 500 mg of synthesized AgNPs and RGO-AgNPs samples (without fabric) were kept wet for 1 h using 2 ml of sweat solution. The entire sample medium was centrifuged at 10,000 rpm for 30 min to obtain precipitate and gently dried in a vacuum oven at 60 °C. Transmission Electron Microscopy (TEM), Techai 20G2-FEI, with an acceleration voltage of 200 kV, was used to examine the nature of particle morphology after dispersing 1 mg of precipitate sample in 20 ml of water using an ultrasonicator for 15 min. The crystal phase transformations of these materials were studied using XRD (D8-ADVANCE PXRD (BRUKER)). An EPR study was also carried out to investigate ($OH^·$) generation from sweat-treated RGO-AgNPs-CT. The sample was tested in the dark for 15 min and immersed in 10 ml of 0.2 M 5,5-dimethyl-1-pyrroline *N*-oxide (DMPO) solution. Thus, the entire medium, including the tested CT, was exposed to sunlight for 15 min after the medium was analyzed using electron paramagnetic resonance spectroscopy (EPR) [28].

Swelling studies

Tested fabrics were immersed in Milli-Q water and sweat solution at 37 °C for swelling measurements. The fabric materials were removed from the medium at appropriate intervals and spread with filter paper to remove excess water before being weighed. Equation (1) was used to calculate the swelling ratio (Q) [29]:

$$\text{Swelling ratio } \mathbf{Q} = \left(\frac{W_t - W_o}{W_o}\right), \quad (1)$$

where W_t is the sample weight at time *t,* and W_o is the initial weight of the CT sample.

Cumulative releases of Ag^+ ion from treated fabric

AAS (Thermo scientific model iCE 3000 series) was used to determine the release of Ag^+ ions from treated fabric samples (AgNPs-CT, RGO-AgNPs-CT, sweat-AgNPs-CT, and sweat-RGO-AgNPs-CT). The CT sample (2×2 cm^2) was immersed in 25 ml of 0.1 M phosphate buffer pH (7.0) at 37 °C with gentle shaking. The 1 ml test sample solution was taken at regular intervals (6, 12, 24, 48, and 72 h) and digested for 30 min with 1 ml of 20% supra nitric acid. The digested solution was subjected to an AAS analysis.

Laundering durability tests

The fabric samples were 50 mm × 150 mm (2.0 × 6.0 in.), and the tested fabric was immersed in a washing solution containing 0.15% w/w local commercial detergent. The samples were stirred mechanically and kept at 50 ± 5 °C for 15 min. The fabrics were then gently squeezed and rinsed with deionized water [30]. The amount of silver on the fabric and its antibacterial activity on the washed fabric was also performed.

Antibacterial activities

Bare and treated fabric samples were evaluated for antibacterial activity using bacterial species viz *E. coli*, *S. aureus* and cellulose-degrading bacterium of *B. subtilis* 5B, personal gift by Santhanam et al. [31]. This bacillus bacterium was found to have active cellulase enzyme activity and isolated from waste cotton fabrics sludge. The preparations of bacterial cultures and fabric samples were evaluated for antibacterial activity by agar diffusion, and the solution suspension method was followed by Dhandapani et al. [32]. In addition, the photoinactivation of sweat-treated CT samples was compared to that of untreated CT samples [33]. The photoinactivation of the experimental setup and sample preparation are provided in supporting information (Fig. S2).

Results and discussion

Preparation of biologically activated ammonia

Ureolytic bacterium of *B. subtilis* (HM475276) was identified for ammonia production from urea-based broth and synthetic urine medium using urease enzyme. As previously reported [28, 33, 34], this bacterium can produce more ammonia from synthetic urine medium. The biological activated ammonia was used for synthesized photocatalyst material of RGO-ZnO nanorod composites and ZnO micro flower to remove the dye and bacterial species under sunlight [28, 33]. S3 depicts the variation of ammonium content in a synthetic urine medium with a *B. subtilis* (HM475276) at regular intervals. In synthetic urine systems, a maximum pH of 10.2 has been noticed in the presence of *B. subtilis*. In comparison, the control system showed no significant change in medium pH. As shown in S3, the production of biologically activated ammonia in synthetic urine medium was estimated at various intervals, and the maximum of biologically activated ammonia was found to be 20,000 ppm. Biologically activated ammonia was used in the photoreduction method to synthesize AgNPs on RGO sheet at the fabric interface.

Morphology observation

Figure 1 depicts FE-SEM images of bare-CT, GO-CT, AgNPs-CT, and RGO-AgNPs-CT. The sample of plain fabric illustrates uniform, neat plain-spun structures with a smooth surface (Fig. 1a). The adsorbed GO sheets on fabric surfaces are shown in Fig. 1b, where the shrinking nature of the cover can be seen. AgNPs with a spherical shape range of 20–50 nm were aggregated and uniformly adhered to CT (Fig. 1c). As shown in Fig. 1d, the photochemical and mild-hydrothermal methods were used to form RGO-AgNPs composite effectively cover the surface with fabric. Furthermore, an enlarged image shows the thick deposition of NPs with RGO sheets on fibres (Fig. 1d). Compared to AgNPs treated on fabric; the RGO sheet provides a platform for the AgNPs ligands. The present results are supported by diffuse reflectance UV–visible spectra, which were then converted into absorption spectra of bare-CT, GO-CT, AgNPs-CT and RGO-AgNPs-CT (Fig. S4). It was displayed that a strong absorption band at 410 nm can be attributed to AgNPs surface plasmon resonance (Fig. S4) [12]. This absorption band was absent on the bare and GO-CT. The UV–visible spectra demonstrated that AgNPs are well deposited on the fabric surface by photoreduction. As a result, the absorption band on the RGO-AgNPs fabric sample was significantly higher than on the AgNPs-CT (Fig. S4). In addition, UV–visible

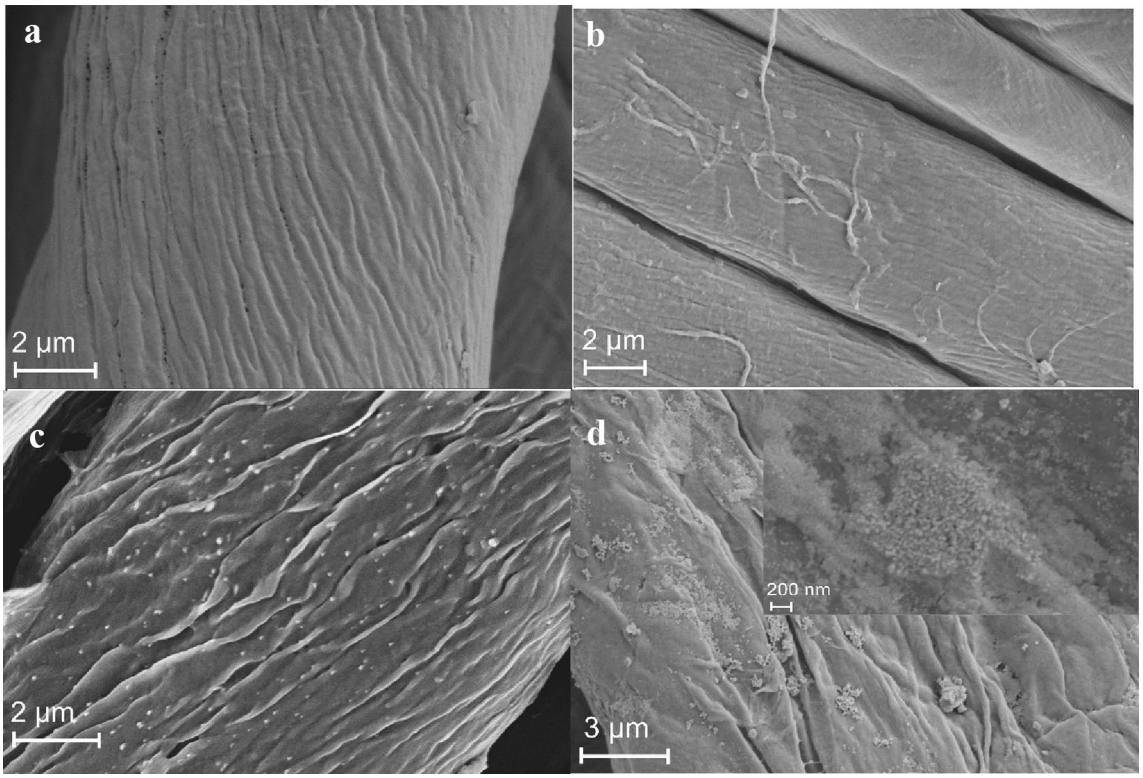

Fig. 1 FE-SEM images of the **a** bare-CT, **b** GO-CT, **c** AgNPs-CT, and **d** RGO-AgNPs-CT. Insets in the enlarged view of FE-SEM image

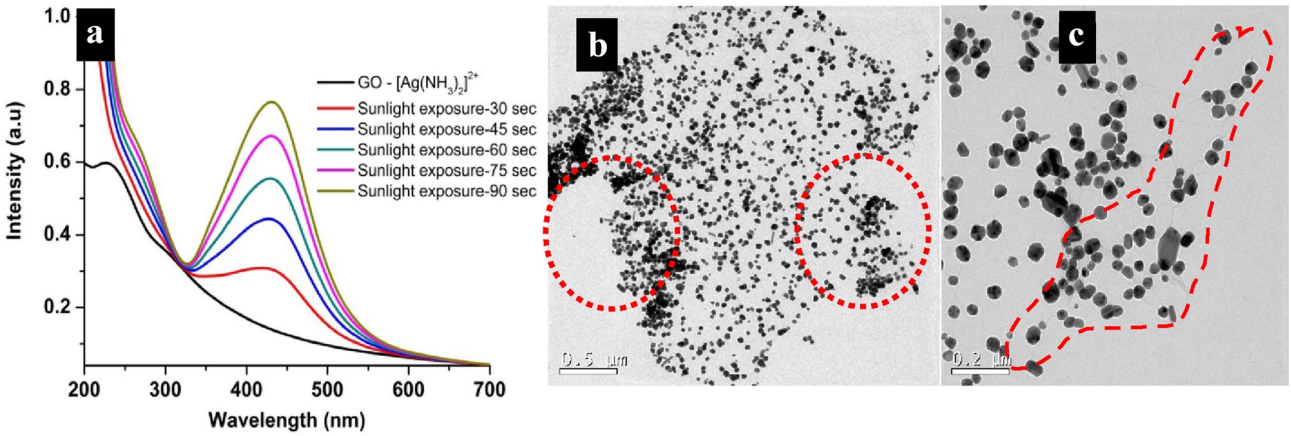

Fig. 2 **a** UV–visible absorption spectra from time-dependent photoreduction of Ag^+ ion into AgNPs on the GO sheet surface by solar simulators illumination time and **b**, **c** TEM images of the RGO-AgNPs

spectroscopy and TEM were used to thoroughly characterize the photoreduction of Ag^+ ions into AgNPs on the GO sheet surface (without fabric). UV–visible absorption spectra from time-dependent photoreduction of Ag^+ ion into AgNPs on the GO sheet surface using solar simulators are shown in Fig. 2a. Under dark conditions, none of the absorption peaks on the GO-$[Ag(NH_3)^2]^{2+}$ were observed. The formation of AgNPs from GO-$[Ag(NH_3)^2]^{2+}$ was attributed to the slight elevation of absorption spectra at 425 nm when exposed to solar simulator light. The maximum absorption band was quietly increased from 30 to 90 s of irradiation time (Fig. 2a). The solar simulator light is adequate for photoreduction of Ag^+ ions into AgNPs on the GO sheet surface at short periods [35]. This sample was also used in the hydrothermal method to analyze the size and shape of AgNPs on the RGO sheet using TEM and revealed the transparency and wrinkles in the RGO sheet (Fig. 2b) which can be provided to the platform of AgNPs formation during the photoreduction method. AgNPs are typically spherically shaped, with an average diameter of 10 to 50 nm. In addition, as noticed, a small nanorod and a few spherical particles were attracted to another particle (Fig. 2c). Most particles were separated and anchored on the RGO sheet with flat deposition by the photoreduction process and then the hydrothermal method [35]. Furthermore, the NPs were aggregated, and the formation of AgNPs was increased on the RGO sheet edges compared to the midpoint region since GO functional groups are more active on the surface of the border than in the interior region, according to the modified hummers method.

XRD

As shown in Fig. 3, the X-ray diffraction patterns were obtained from bare-CT, AgNPs-CT, GO-CT, and RGO-AgNPs-CT. Diffraction peaks of bare-CT were observed at

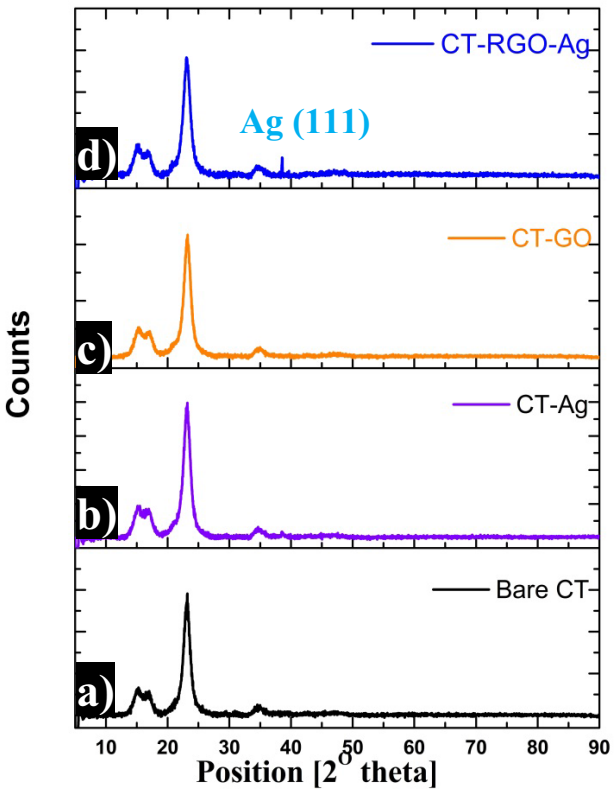

Fig. 3 XRD patterns of the **a** bare-CT, **b** AgNPs-CT, **c** GO-CT, and **d** RGO-AgNPs-CT

2θ values of 14.64°, 16.51°, 22.31°, and 34.08°, respectively [36]. A comparable XRD pattern was noticed in GO-CT (Fig. 3a, c). Furthermore, the diffraction peak at 38.5° corresponds to the face of the centre cubic phase of Ag (111), which corresponds to JCPDs nos. 89-1397. A low peak signal at a 2θ value of 38.5° was obtained after treating fabrics

with AgNPs and RGO-AgNPs, indicating a lower weight fraction of silver in the fabric surface (Fig. 3b, d). Besides, the fabric sample had an undetectable oxidized silver crystal phase. It demonstrates that AgNPs are effectively synthesized on the RGO sheet at the fabric surface by photoreduction followed by a mild-hydrothermal process.

XPS

XPS investigated the binding energy of C1*s* and Ag3*d* in the RGO-AgNPs-CT and GO samples. The C1*s* XPS spectrum of GO at 280–292 eV in Fig. 4a showed the characteristic peaks of C–C, C–OH, C–O–C, C=O, and O–C=O, which can be attributed to the presence of epoxy, hydroxyl, and carbonyl groups, respectively [37]. According to Fig. 4b, the RGO-AgNPs-CT sample significantly decreased the intensity of C1*s* related to oxygenated functional groups (C–O–H and C–O–C). The photoreduction process, followed by a mild-hydrothermal method, confirmed that it removed most of the epoxide, hydroxyl, and carbonyl functional groups. The presence of two binding energies for Ag3d in the RGO-AgNPs sample, 368.1 and 374.1 eV, with a 6.0 eV difference, proved metallic silver formation [37]. The difference in the binding energies is about 6.0 eV, attributed to the electron transfer between AgNPs and RGO.

TGA

TGA was used to characterize the thermal properties of bare-CT, AgNPs-CT, GO-CT, and RGO-AgNPs-CT, as shown in Fig. 4d. The elimination of adsorbed moisture content from the fabric surface resulted in a preliminary weight loss of 1.4% at 84.94 °C for the plain fabric. A significant portion of weight loss in the fabric was observed with a temperature rise from 311.73 °C to 498.00 °C due to thermal degradation. Furthermore, the weight loss plot was relatively high. The decomposition of carbon material from GO and RGO occurred on the GO-CT, and RGO-AgNPs-CT samples at temperatures ranging from 361.25 to 520.00 °C [38]. TGA spectra show that the AgNPs on RGO and the plain cotton fabric contributed 8.9% and 4.5% of the final weight, respectively. Furthermore, the presence of RGO increased the residue content on the RGO-AgNPs treated fabric compared to the bare-CT, AgNPs-CT, and GO-CT samples due to the RGO sheet providing a platform for the AgNPs ligands on the fabric surface.

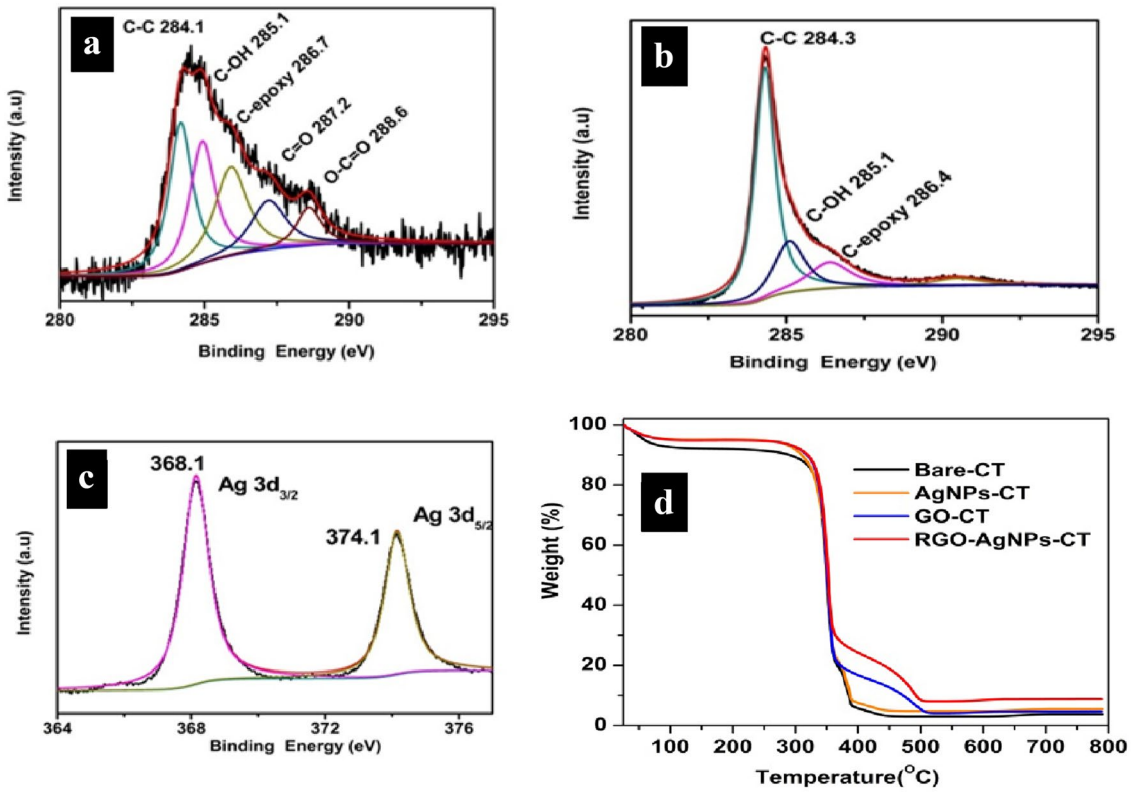

Fig. 4 XPS spectra of the **a** C1*s* of GO, **b** C1*s* of RGO-AgNPs-CT, **c** Ag3d of RGO-AgNPs-CT, and **d** TGA spectra of the bare-CT, AgNPs-CT, GO-CT, RGO-AgNPs-CT

RGO sheets were used as the AgNPs and fabric interface layer in this study. The GO sheet is physically adsorbent to the fabric surface. $[Ag(NH_3)^2]^{2+}$ ion affinity fabric and GO sheet surfaces such as hydroxyl, epoxide, carbonyl, and carboxyl groups by electrostatic interaction [35, 39]. This electrostatic fixation area depends on the loading/formation of silver nanocrystals on the GO sheet at the fabric surface. Direct light reduced the $[Ag(NH_3)^2]^{2+}$ complex to the formation of the silver nanocrystal [35, 39]. Thus, photoreduction occurred on GO sheets with the cotton fabric surface, resulting in stable GO-AgNPs nanocomposites. XPS analysis confirms the formation of RGO-AgNPs from the GO-$[Ag(NH_3)^2]^{2+}$ ion complex via photoreduction followed by the hydrothermal method. TGA and diffuse reflectance UV–visible spectra revealed an increase in silver loading on the RGO-AgNPs treated fabric. This finding supports the observation made by Golsheikh et al. [40].

Sweat interference study

The antibacterial properties of nanomaterials incorporated into the CT samples were applied to the mildly injured skin surface for long-term protection from bacterial infections until tissue regeneration or tissue repair on the skin. However, the release of AgNPs on cotton fabric is affected by free Cl^- ions and temperature [22, 23]. A substantial amount of NaCl is present in sweat [23]. This study exposed treated fabric to sweat for 1 h to investigate the silver dissolution rate, EDAX-Elemental mapping, intermediated changes in crystal phase, and particle morphology using XRD and TEM. The durability test was performed on washing cycles to correlate with antibacterial activity.

The swelling tests for bare and treated fabric samples were performed from Milli-Q water and sweat solution at various time intervals, as shown in Fig. 5a. The swelling rates of the bare-CT, GO-CT, AgNPs-CT, and RGO-AgNPs-CT were lower in the Milli-Q water than in the sweat solution. The swelling rate of bare-CT was 5.2 after 1 min of contact with sweat solution and expanded to about 5.5 after 60 min. The swelling ratios of GO-CT, AgNPs-CT, and RGO-AgNPs-CT were found to be 6.7, 8.0, and 6.9, respectively. It can be due to the water feasting and Cl^- ion adsorption on the surface of the cotton fabric by AgNPs. As a result of the RGO sheet's presence, the swelling rate is moderate.

Figure 5b depicts the cumulative release of Ag^+ ion profiles from AgNPs-CT, RGO-AgNPs-CT, sweat-AgNPs-CT, sweat-RGO-AgNPs-CT samples under solution suspended conditions at various time intervals. The original silver content of fabric samples treated with AgNPs and RGO-AgNPs was 8.0 and 14.5 ppm, respectively. The AgNPs-CT sample showed a gradual increase in Ag^+ ion release at 72 h intervals (4.0 ppm). At 72 h, an RGO-AgNPs-C sample released 7.5 ppm of Ag^+ ion (Fig. 5b). During sweat treatment of the fabric sample, the Ag^+ ion was released at around 2 (Sweat-AgNPs-CT) and 2.5 ppm (Sweat-RGO-AgNPs-CT). Sweat solution affects the rate at which AgNPs dissolve from treated fabric in this study. Levard et al. [21] observed a higher rate of silver dissolution in the presence of NaCl at 0.1 M during a solution suspension study. The kinetic model was also developed based on the silver dissolution rate in environmental water stimulation [21]. In the present study, the silver dissolution rate on the tested AgNPs and RGO-AgNPs fabric in sweat solution were lower in the wet condition due to the formation of AgCl on the fabric; sweat reduces the dissolution rate of Ag^+ ions [22].

Figure 6 shows EDAX-Elemental mapping for sweat-AgNPs-CT and sweat-RGO-AgNPs-CT, which correspond to the contrast distribution of the C, O, Ag, and Cl elements. According to the elemental mapping, the sweat-treated fabric surface uniformly absorbed the Cl element. Besides, Cl

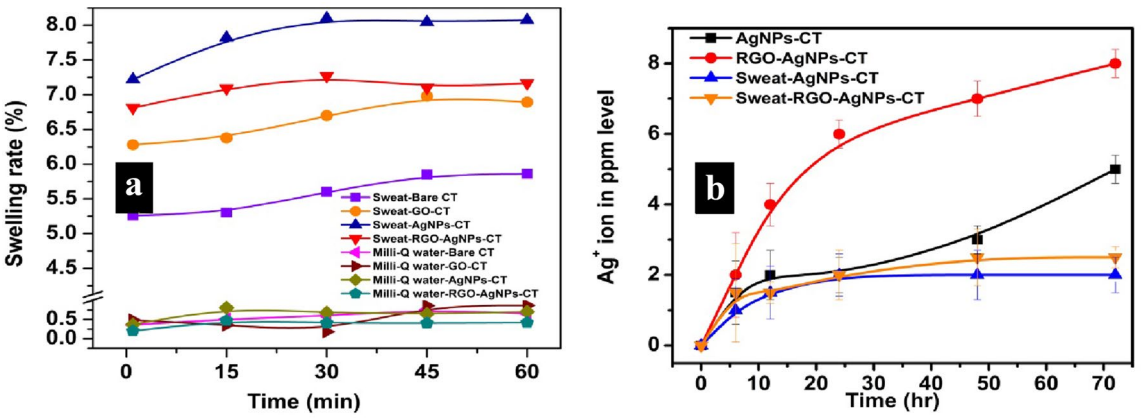

Fig. 5 **a** Swelling tests for bare and treated cotton fabric samples were carried out from Milli-Q water and sweat solution at various time intervals, and **b** cumulative releasing of Ag^+ ion profiles from AgNPs-CT, RGO-AgNPs-CT, Sweat AgNPs-CT, and Sweat-RGO-AgNPs-CT under aqueous solution suspended conditions at different time intervals

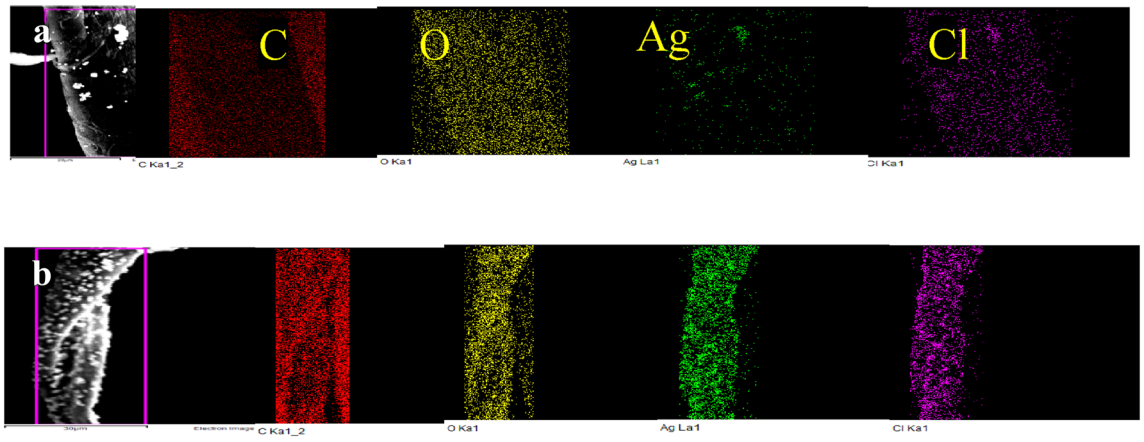

Fig. 6 EDAX-Elemental mapping of **a** sweat-AgNPs-CT and **b** sweat-RGO-AgNPs-CT

element mapping of AgNPs and RGO-AgNPs treated fabric sample has better colour contrast with an Ag element (Fig. 6a, b), indicating more Cl^- ion interaction with a sweat-RGO-AgNPs-CT sample corresponding to Ag/AgCl formation. Furthermore, owing to the vast space between the cotton thread matrix and the absorbed Cl^- ion content from sweat solution [19, 22], the fabric can increase the dissolved oxygen from the air. These two conditions favour the formation of Ag/AgCl on the fabric surface [22].

Furthermore, RGO was loaded onto the fabric with a low concentration of AgNPs. It is unable to investigate changes in the crystal phase and particle shape in sweat solution. As a result, we performed comparable experiments for sweat interaction with nanomaterials (AgNPs and RGO-AgNPs) for 1 h in a wet environment without fabric. XRD pattern of RGO-AgNPs with and without sweat treated as shown in Fig. S5. The relative intensity of Ag was slight changes on the sweat-RGO-AgNPs sample compared to RGO-AgNPs. In addition, diffraction peaks of sweat-RGO-AgNPs were observed at 2θ values of 27.82°, 32.24°, 46.21°, 54.94°, and 57.61°, respectively, attributed to the lattice planes of (111), (200), (220), (311), and (222), which are the related cubic lattice of AgCl (JCPDS no. 31-1238). XRD pattern confirmed the Ag/AgCl crystal phase formation on sweat-RGO-AgNPs compared to RGO-AgNPs. This significance was visualized as the particle morphology changed from spherical to cubic shape (Fig. S6) with increasing particle size distribution from 100 to 350 nm, thus compared with Milli-Q water treated sample. The presence of Cl^- ions as a significant portion in sweat solution involved the primary contribution of Ag/AgCl formation [22, 23]. According to the earlier report [19–22], the material transition of Ag/AgCl from AgNPs depends on the presence of Cl^- ions, dissolved oxygen, the size and shape of AgNPs, naturally occurring organic matter, and the medium pH. Furthermore, the sweat-RGO-AgNPs-CT sample was subjected to EPR spectroscopy in the presence of 0.2 M DMPO solution with sunlight exposure compared to the dark conditions (Fig. S7). The four distinct peaks were associated with $OH^{\cdot}$ radicals generation from sweat-RGO-AgNPs-CT under sunlight illumination after 15 min (Fig. S7). However, the dark condition of the sample was exhibited by the absence of four distinct peaks on the EPR spectra. These findings agreed with previous research on the photocatalytic behaviour of RGO-Ag/AgCl nanomaterials [41, 42]. The sweat-RGO-AgNPs-CT sample has a greater potential of generating $OH^{\cdot}$ radicals in response to sunlight exposure, which can help with the photoinactivation of bacterial growth and prevent the formation of biofilms.

Antibacterial activity

Antibacterial activity of bare-CT, GO-CT, AgNPs-CT, RGO-AgNPs-CT, ST-bare-CT, ST-GO-CT, ST-AgNPs-CT, and ST-RGO-AgNPs-CT samples against *E. coli*, *S. aureus*, and *B. subtilis* 5B was examined by the agar diffusion method and solution suspension studies. The present results have been tabulated and presented in Table 1 AgNPs treated

Table 1 Antibacterial activity of treated and untreated cotton fabric samples by agar diffusion method

S. no.	Fabric samples	Antibacterial inhibition zone (mm)		
		E. coli	*S. aureus*	*B. subtilis* 5B
1	Bare-CT	–	–	–
2	GO-CT	–	–	–
3	AgNPs-CT	6.4 ± 0.2	3.2 ± 0.1	2.1 ± 0.1
4	RGO-AgNPs-CT	4.5 ± 0.2	2.8 ± 0.1	2.0 ± 0.1
5	ST-GO-CT	–	–	–
6	ST-AgNPs-CT	3.0 ± 0.1	2.0 ± 0.1	1.0 ± 0.1
7	ST-RGO-AgNPs-CT	3.5 ± 0.1	1.2 ± 0.1	1.0 ± 0.1

fabric sample formed a significantly larger inhibition zone than RGO-AgNPs-CT and GO-CT due to the dependence upon the release of Ag^+ ions [20, 21]. *S. aureus* has a smaller area of inhibition than *E. coli* [32]. Furthermore, we noticed that the treated fabric samples have excellent antibacterial activity against the cellulose-degrading bacterium *B. subtilis* 5B. Antibacterial agar diffusion studies revealed the following pattern: AgNPs-CT>RGO-AgNPs-CT>ST-AgNPs-CT>ST-RGO-AgNPs-CT>ST-GO-CT>GO-CT. Besides, while treating sweat, the antibacterial inhibition zone was lower when compared to without sweat (Table 1). For the antibacterial activity studied by solution suspension studies (Fig. 7), RGO-AgNPs-CT exhibited the highest reduction of bacterial survival rate when compared to AgNPs-CT and GO-CT against the bacterial species *E. coli* (12 h), *S. aureus* (24 h), and *B. subtilis* 5B (24 h), respectively. The reduction of bacterial survival rate of ST-RGO-AgNPs-CT, ST-AgNPs-CT, and ST-GO-CT was lower than RGO-AgNPs-CT, AgNPs-CT, and GO-CT, respectively. The formation of an Ag/AgCl bridge inhibits the antibacterial activity reported by Chambers et al. [43]. The antibacterial solution suspension studies revealed the following trend: RGO-AgNPs-CT>ST-RGO-AgNPs-CT>AgNPs-CT>ST-AgNPs-CT>ST-GO-CT>GO-CT.

Since RGO-AgNPs-CT and ST-RGO-AgNPs-CT have excellent antibacterial activity in solution suspension, we used them to photoinactivation the *E. coli* bacterium under sunlight. XRD spectra and FE-SEM images confirmed the material transformation of Ag/AgCl on the ST-RGO-AgNPs-CT fabric by the effect of sweat. According to the present study, sweat environment changes in the material transformation of RGO-Ag/AgCl-CT to perform admirably

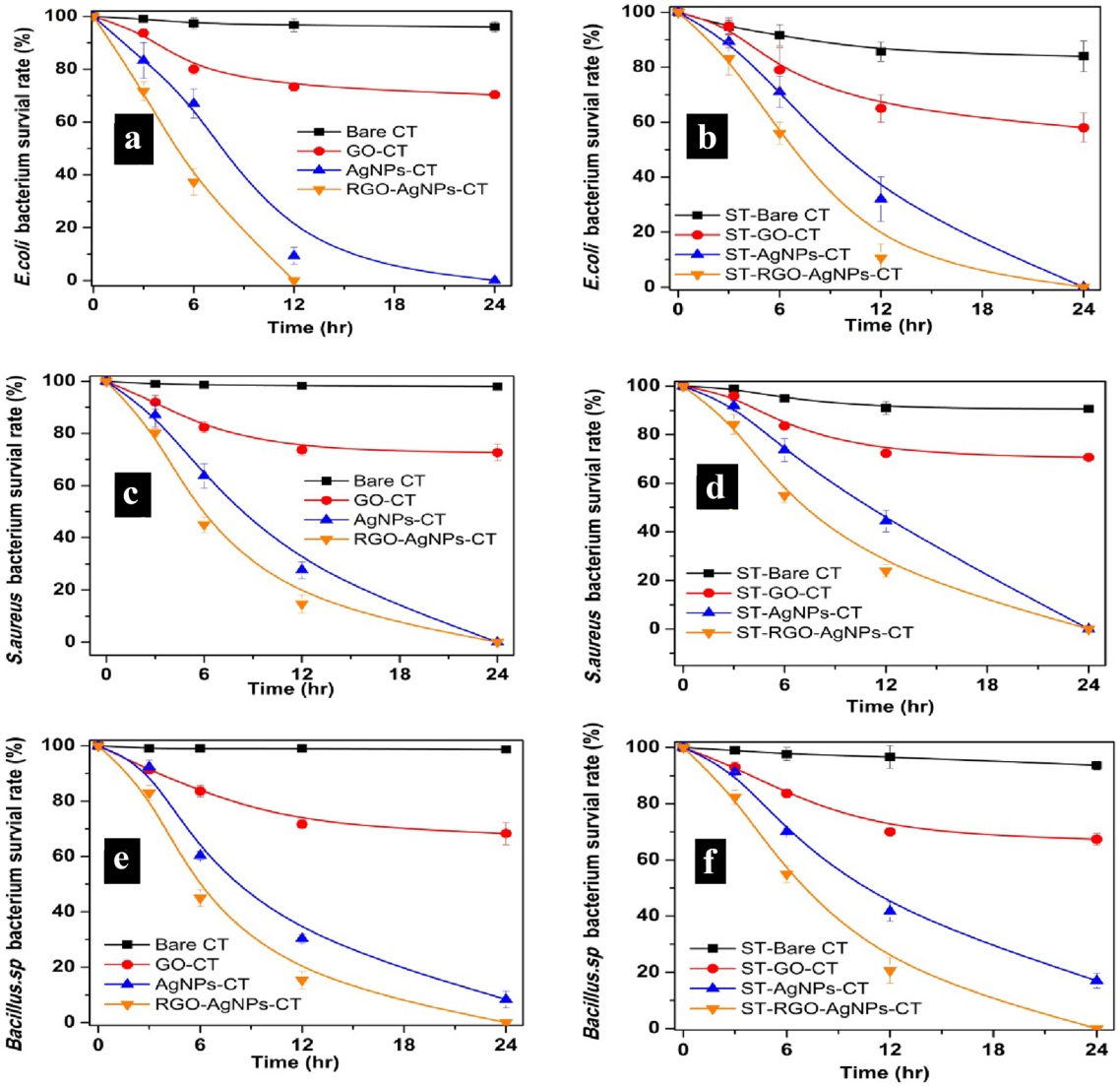

Fig. 7 Antibacterial activity of tested cotton fabric samples under solution suspension condition against *E. coli*, *S. aureus*, and *B. subtilis* 5B

in sunlight and are appropriate for biomedical textile technology. The Ag/AgCl nanomaterial has a high potential for generating $OH^{\cdot}$ radicals under the influence of sunlight, which can be used to degrade a wide range of organic pollutants [44, 45]. Several researchers have focused on the Ag/AgCl composite to eliminate bacterial species from contaminated water under illumination [46, 47]. The falling bacterial survival rate on the photoreactor medium during the photocatalytic experiment in the presence of a tested fabric under sunlight at various time intervals (Fig. 8). The bacterial survival rate was entirely reduced after 45 min of sunlight exposure. This observation confirmed the decrease in bacterial survival rate caused by the generation of $OH^{\cdot}$ radicals from the RGO-Ag/AgCl particle surface on the fabric [41]. After 60 min in darkness, a sustained bacterial survival rate was noticed. The results demonstrated that ST-RGO-AgNPs-CT have excellent antibacterial properties compared to RGO-AgNPs-CT. In addition, a Lux meter was also used to measure and record sunlight intensity during photocatalytic experiments at regular time intervals (Fig. S8). The profile of sunlight intensity fluctuation is caused by cloudy interference at the geographical location site (where that place operated photocatalytic experiment). The total viable bacterial count method confirmed that increasing the intensity of sunlight corresponds to gradually decreasing the bacterial survival rate (Fig. S8). After 45 min of exposure to sunlight, none of the bacterial colonies enrichment on the petri plate. As a result, the effect of sunlight intensity is critical in the generation of $OH^{\cdot}$ from the RGO-Ag/AgCl overcoated fabric surface [41, 44]. Furthermore, sweat-treated RGO-AgNPs-CT was used to capture the epi-fluorescent microscopic features of *E. coli* cells at regular intervals (Fig. S9). Living cells are green, while dead cells are red. In the dark, it represents green-stained living bacteria cells. The disintegration of *E. coli* cells in the photocatalytic reactor was noticeable after 45 min of exposure to sunlight, as indicated by the red colour. This finding could be elucidated by the fact that the contact distance between sweat-treated RGO-AgNPs-CT and *E. coli* cells influences reactive oxygen radical species in the presence of sunlight [32, 33]. EPR findings also support the present investigation.

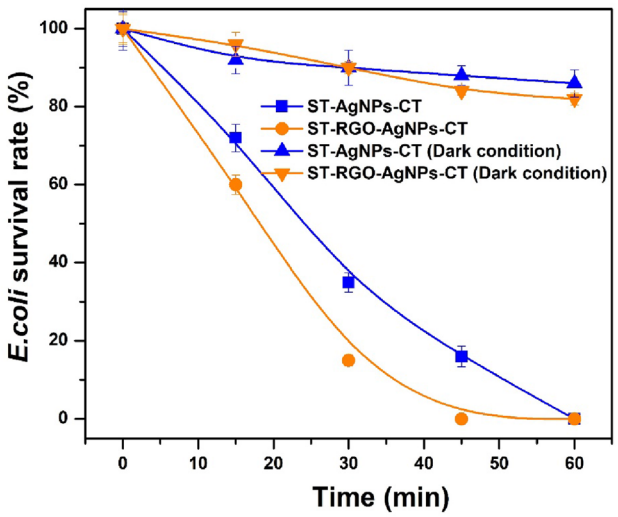

Fig. 8 *E. coli* bacterium survival rate on the sweat-treated RGO-AgNPs and AgNPs fabric under sunlight exposure time for 60 min at solution suspension condition and compared to the dark condition were, respectively

It is possible to explain the photoinactivation of *E. coli* bacterium survival rate by ST-RGO-AgNPs on the fabric surface under sunlight. The fabric sample was exposed to sunlight, followed by Ag/AgCl on the RGO sheet as an active photocatalyst [44, 45]. Light-harvesting of the visible light region by Ag/AgCl particles from the natural abundance of sunlight [44] and RGO nanosheet capable of electron–hole separation. Visible light excites the Ag/AgCl NPs surface, and this coherent oscillation of electrons produces and reacts with water molecules to produce hydroxyl radicals [45]. Furthermore, photoexcited electrons from Ag/AgCl NPs were transferred to the surface of the RGO sheet. These electrons have the potential to react with dissolved oxygen, producing reactive oxygen species [44, 45]. These radicals are involved in the cleavage of *E. coli* cells, resulting in a decrease in bacterial survival rate over time intervals [46, 47]. The entire photocatalytic process was carried out on the surface of the cotton fabric under sunlight. The production of $OH^{\cdot}$ radicals may be affected by the concentration of RGO-Ag/AgCl on the cotton fabric as a result of Ag/AgCl acting as a trigger on visible light absorption and being accelerated by photoexcited electron–hole pairs. As a result, Ag/AgCl particles are found on the cotton fabric and nearby *E. coli* cells. Xia et al. reported that synthesized Ag/AgCl on the RGO material surface achieved the inactivation of *E. coli* bacterium cells (2.0×10^7 CFU/ml) within 25 min of visible light (9.3 mW/cm^2) via Ag^+ ions and reactive oxygen species [48]. Cheikhrouhou et al. demonstrated that cotton fabrics decorated with Ag/AgCl had higher inactivation of *E. coli* and *S. aureus* (1.5×10^7 CFU/ml) after 15 min of 100 W Xenon lamp exposure than Ag/AgBr due to efficient generation of reactive oxygen species [49]. From that discussion, ST-RGO-AgNPs cotton fabric could be an effective photocatalyst for deactivating *E.coli* bacterium (6.4×10^6 CFU/ml) at 45 min by photocatalytic effect. The present study examined the interaction between bacterial cells and a graphene-based photocatalyst coated on fabric to understand photoinactivation mechanisms.

The textile finishing considered the material stability on the cotton fabric surface. In this study, the AgNPs wiped out on the treated cotton fabric by sweat solution and washed cycles with local detergent were investigated.

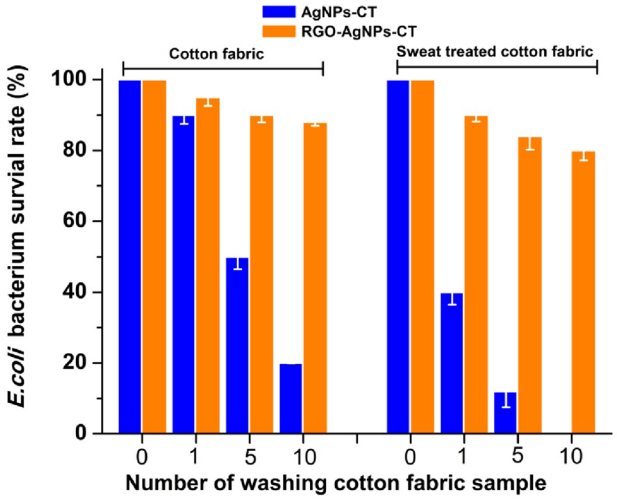

Fig. 9 Antibacterial activity of tested fabric samples versus number of washing cycles

As a result, we participated in numerous washing cycles on the cotton fabric sample to determine the amount of silver content and antibacterial activity after 5 and 10th washes in liquid detergent, as shown in Fig. 9. Sweat-treated and untreated fabric samples both had a minimum survival rate of 12–24 h. However, there is a significant variation in bacterial survival rate during the first 0–12 h due to fabric interacting with bacterial cells or the silver ion releasing factor, as noted in the solution suspension study. There is a significant loss of silver loading content between 3 and 4 ppm after 5 and 10th times repeated washing of fabric sample with AgNPs in the presence of sweat treated compared to untreated sample (1 and 3 ppm). After the 10th washes, the silver loss from RGO-AgNPs was 2 ppm (Fig. 9). Despite this, the sweat-treated RGO-AgNPs fabric sample demonstrated excellent retention in bacterial survival reduction with lower silver dissolution at the 10th cycle of laundry durability tests when compared to the sweat-treated AgNPs fabric sample due to the presence of Ag/AgCl on the fabric and less interaction with NPs during the washing process [23]. The presence of RGO is favourable in the wrapping with fabric surface with improved AgNPs loading and material stability from laundry durability tests. Besides, sweat environment changes in the material transformation of RGO-Ag/AgCl-CT were developed as a perfect photocatalyst for eliminating contaminated bacterial species via $OH^{\cdot}$ radicals. The present results can aid with antibacterial testing of fabric samples that come into touch with the skin and influence the sweat environment. In addition, graphene coating on cloth or an electronic gadget for health monitoring with an antibacterial surface protects against bacterial infections.

Conclusions

In the present work, the RGO-AgNPs on the fabric surfaces were prepared by facile bio-approach combined with photoreduction and hydrothermal technique, and the antibacterial activity examined sweat interference with and without treated cotton fabric samples. The formation of RGO from the reduction process of GO during the hydrothermal reaction was described in XPS. FE-SEM revealed the formation of AgNPs (10–50 nm) on the RGO sheet with CT. In addition, UV–visible spectra and TEM images confirmed the formation of AgNPs on RGO sheets. The TGA shows that CT treated with RGO-AgNPs had more silver (8%) than AgNPs-CT due to the RGO sheet providing a more platform for the AgNPs ligands. The results of the XRD, EDAX elemental mapping, and AAS revealed that sweat solution promoted the formation of Ag/AgCl on the fabric and suppressed the release of Ag^{+} ions from treated CT. Compared to the agar diffusion method, the RGO-AgNPs-CT has excellent antibacterial activity in the solution suspension. However, sweat interference treated cotton fabric has reduced antibacterial activity against *E. coli*, *S. aureus*, and *B. subtilis* 5B due to Ag/AgCl developments on the CT. Furthermore, the RGO-Ag/AgCl has a perfect photocatalyst for eliminating *E. coli* via $OH^{\cdot}$ radicals. According to the present study, fabric samples treated with RGO-Ag/AgCl by sweat to perform admirably in sunlight and are appropriate for biomedical textile technology. In addition, further study is also required to explore the biocompatibility and antimicrobial surface of graphene-coated fabrics, as well as the development of health monitoring devices, which should be a focus of future research.

Supplementary Information The online version contains supplementary material available at https://doi.org/10.1007/s00449-022-02789-7.

Acknowledgements The authors are grateful to the Researchers Supporting Project No. (RSP-2021/398), King Saud University, Riyadh, Saudi Arabia. Dr. P. Dhandapani thanks to D.S. Kothari postdoctoral Fellowship (Normal) (File No. F.4-2/2006 (BSR) BL/17-18/0343) by University Grants Commission (UGC), New Delhi, India.

Author contributions Perumal Dhandapani: Experimental work, Field collection, Writing—original draft. Santhoshkumar Murali: Methodology. Jayaraman Narenkumar: Validation, Result Interpretation. Mohamad S. AlSalhi: Resources, Funding acquisition, Writing—review and editing. Paulraj Arun Kumar: Validation, Result Interpretation, Writing—review and editing. Sandhanasamy Devanesan: Validation, Formal analysis, Writing—review and editing. Seenivasan Kokilaramani: Writing—review and editing, Aruliah Rajasekar: Project administration, Supervision, Validation, Writing—review and editing.

Declarations

Conflict of interest The authors declare that they have no conflict of interest.

References

1. Shahriari-Khalaji M, Alassod A, Nozhat Z (2022) Cotton-based health care textile: a mini review. Polym Bull. https://doi.org/10.1007/s00289-021-04015-y
2. Sanders D, Grunden A, Dunn RR (2021) A review of clothing microbiology: the history of clothing and the role of microbes in textiles. Biol Lett 17(1):20200700. https://doi.org/10.1098/rsbl.2020.0700
3. Bhandari V, Jose S, Badanayak P, Sankaran A, Anandan V (2022) Antimicrobial finishing of metals, metal oxides, and metal composites on textiles: a systematic review. Ind Eng Chem Res 61(1):86–101. https://doi.org/10.1021/acs.iecr.1c04203
4. Subramanian B, Priya KA, Rajan ST, Dhandapani P, Jayachandran M (2014) Antimicrobial activity of sputtered nanocrystalline CuO impregnated fabrics. Mater Lett 128:1–4. https://doi.org/10.1016/j.matlet.2014.04.056
5. Pachaiappan R, Rajendran S, Show PL, Manavalan K, Naushad M (2020) Metal/metal oxide nanocomposites for bactericidal effect: a review. Chemosphere. https://doi.org/10.1016/j.chemosphere.2020.128607
6. Gao YN, Wang Y, Yue TN, Weng YX, Wang M (2021) Multifunctional cotton non-woven fabrics coated with silver nanoparticles and polymers for antibacterial, superhydrophobic and high-performance microwave shielding. J Colloid Interface Sci 582:112–123. https://doi.org/10.1016/j.jcis.2020.08.037
7. Karuppusamy S, Pratheepkumar A, Dhandapani P, Maruthamuthu S, Kulandainathan MA (2015) A strategy to develop bioactive nanoarchitecture cellulose: sustained release and various applications. J Biomed Nanotechnol 11(9):1535–1549. https://doi.org/10.1166/jbn.2015.2049
8. Babu KF, DhandapaniP MS, Kulandainathan MA (2012) One pot synthesis of polypyrrole silver nanocomposite on cotton fabrics for multifunctional property. Carbohydr Polym 90(4):1557–1563. https://doi.org/10.1016/j.carbpol.2012.07.030
9. Montazer M, ShameiA AF (2014) Synthesis of nanosilver on polyamide fabric using silver/ammonia complex. Mater Sci Eng C 38:170–176. https://doi.org/10.1016/j.msec.2014.01.044
10. Kwak WG, Oh MH, Gong MS (2015) Preparation of silver-coated cotton fabrics using silver carbamate via thermal reduction and their properties. Carbohydr Polym 115:317–324. https://doi.org/10.1016/j.carbpol.2014.08.070
11. Montazer M, Alimohammadi F, Shamei A, Rahimi MK (2012) In situ synthesis of nano silver on cotton using Tollens' reagent. Carbohydr Polym 87(2):1706–1712. https://doi.org/10.1016/j.carbpol.2011.09.079
12. Dhandapani P, Devanesan S, Arulprakash A, AlSalhi MS, Paramasivam S, Rajasekar A (2020) Bio-approach synthesis of nanosilver impregnation on calcium hydroxyapatite by biological activated ammonia from urinary waste. Arab J Chem 13(6):5878–5889. https://doi.org/10.1016/j.arabjc.2020.04.024
13. Olga M, Jana M, Anna M, Irena K, Jan M, Alena Č (2022) Antimicrobial properties and applications of metal nanoparticles biosynthesized by green methods. Biotechnol Adv. https://doi.org/10.1016/j.biotechadv.2022.107905
14. Siddiqi KS, Husen A, Rao RA (2018) A review on biosynthesis of silver nanoparticles and their biocidal properties. J Nanobiotechnol 16(1):1–28. https://doi.org/10.1186/s12951-018-0334-5
15. Velmurugan P, Cho M, Lee SM, Park JH, Bae S, Oh BT (2014) Antimicrobial fabrication of cotton fabric and leather using green-synthesized nanosilver. Carbohydr Polym 106:319–325. https://doi.org/10.1016/j.carbpol.2014.02.021
16. Balakumaran MD, Ramachandran R, Jagadeeswari S, Kalaichelvan PT (2016) In vitro biological properties and characterization of nanosilver coated cotton fabrics—an application for antimicrobial textile finishing. Int Biodeterior Biodegrad 107:48–55. https://doi.org/10.1016/j.ibiod.2015.11.011
17. Durán N, Durán M, De Jesus MB, Seabra AB, Fávaro WJ, Nakazato G (2016) Silver nanoparticles: a new view on mechanistic aspects on antimicrobial activity. Nanomed Nanotechnol Biol Med 12(3):789–799. https://doi.org/10.1016/j.nano.2015.11.016
18. Ahmad SA, Das SS, Khatoon A, Ansari MT, Afzal M, Hasnain MS, Nayak AK (2020) Bactericidal activity of silver nanoparticles: a mechanistic review. Mater Sci Energy Technol 3:756–769. https://doi.org/10.1016/j.mset.2020.09.002
19. Zhang W, Xiao B, Fang T (2018) Chemical transformation of silver nanoparticles in aquatic environments: mechanism, morphology and toxicity. Chemosphere 191:324–334. https://doi.org/10.1016/j.chemosphere.2017.10.016
20. Pareek V, Gupta R, Panwar J (2018) Do physico-chemical properties of silver nanoparticles decide their interaction with biological media and bactericidal action? A review. Mater Sci Eng C 90:739–749. https://doi.org/10.1016/j.msec.2018.04.093
21. Levard C, Mitra S, Yang T, Jew AD, Badireddy AR, Lowry GV, Brown Jr GE (2013) Effect of chloride on the dissolution rate of silver nanoparticles and toxicity to *E. coli*. Environ Sci Technol 47(11):5738–5745. https://doi.org/10.1021/es400396f
22. Wagener S, Dommershausen N, Jungnickel H, Laux P, Mitrano D, Nowack B, Schneider G, Luch A (2016) Textile functionalization and its effects on the release of silver nanoparticles into artificial sweat. Environ Sci Technol 50(11):5927–5934. https://doi.org/10.1021/acs.est.5b06137
23. Hedberg J, Skoglund S, Karlsson S, Wold MES, OdnevallWallinder I, Hedberg Y (2014) Sequential studies of silver released from silver nanoparticles in aqueous media simulating sweat, laundry detergent solutions and surface water. Environ Sci Technol 48(13):7314–7322. https://doi.org/10.1021/es500234y
24. Dasari Shareena TP, McShan D, Dasmahapatra AK, Tchounwou PB (2018) A review on graphene-based nanomaterials in biomedical applications and risks in environment and health. Nano-micro Lett 10(3):1–34. https://doi.org/10.1007/s40820-018-0206-4
25. Han W, Wu Z, Li Y, Wang Y (2019) Graphene family nanomaterials (GFNs)—promising materials for antimicrobial coating and film: a review. Chem Eng J 358:1022–1037. https://doi.org/10.1016/j.cej.2018.10.106
26. Kumar S, Chatterjee K (2016) Comprehensive review on the use of graphene-based substrates for regenerative medicine and biomedical devices. ACS Appl Mater Interfaces 8(40):26431–26457. https://doi.org/10.1021/acsami.6b09801
27. Molina J (2016) Graphene-based fabrics and their applications: a review. RSC Adv 6:68261–68291. https://doi.org/10.1039/C6RA12365A
28. Dhandapani P, AlSalhi MS, Karthick R, Chen F, Devanesan S, Kim W (2021) Biological mediated synthesis of RGO-ZnO composites with enhanced photocatalytic and antibacterial activity. J Hazard Mater 409:124661. https://doi.org/10.1016/j.jhazmat.2020.124661
29. Ehsani A, Asefnejad A, Sadeghianmaryan A, Rajabinejad H, Chen X (2021) Fabrication of wound dressing cotton nano-composite coated with Tragacanth/Polyvinyl alcohol: Characterization and in vitro studies. ECS J Solid State Sci Technol 10(1):013002. https://doi.org/10.1149/2162-8777/abdc4c
30. Gao F, Mi Y, Wu X, Yao J, Qi Q, Chen W, Cao Z (2022) Preparation of quaternized chitosan/Ag composite nanogels in inverse miniemulsions for durable and antimicrobial cotton fabrics. Carbohydr Polym 278:118935. https://doi.org/10.1016/j.carbpol.2021.118935
31. Santhanam M, Selvaraj R, Annamalai S, Sundaram M (2017) Combined electrochemical, sunlight-induced oxidation and biological process for the treatment of chloride containing textile

effluent. Chemosphere 186:1026–1032. https://doi.org/10.1016/j.chemosphere.2017.08.066
32. Dhandapani P, Siddarth AS, Kamalasekaran S, Maruthamuthu S, Rajagopal G (2014) Bio-approach: ureolytic bacteria mediated synthesis of ZnO nanocrystals on cotton fabric and evaluation of their antibacterial properties. Carbohydr Polym 103:448–455. https://doi.org/10.1016/j.carbpol.2013.12.074
33. Dhandapani P, Devanesan S, Narenkumar J, Maruthamuthu S, AlSalhi MS, Rajasekar A, Ahamed A (2020) Novel synthesis of ZnO by Ice-cube method for photo-inactivation of E. coli. Saudi J Biol Sci 27(4):1130–1138. https://doi.org/10.1016/j.sjbs.2020.02.005
34. Dhandapani P, Prakash AA, AlSalhi MS, Maruthamuthu S, Devanesan S, Rajasekar A (2020) Ureolytic bacteria mediated synthesis of hairy ZnO nanostructure as photocatalyst for decolorization of dyes. Mater Chem Phys 243:122619. https://doi.org/10.1016/j.matchemphys.2020.122619
35. Zhang Y, Yuan X, Wang Y, Chen Y (2012) One-pot photochemical synthesis of graphene composites uniformly deposited with silver nanoparticles and their high catalytic activity towards the reduction of 2-nitroaniline. J Mater Chem 22(15):7245–7251. https://doi.org/10.1039/C2JM16455H
36. Mia R, Sk MS, Oli ZBS, Ahmed T, Kabir S, Waqar MA (2021) Functionalizing cotton fabrics through herbally synthesized nanosilver. Clean Eng Technol 4:100227. https://doi.org/10.1016/j.clet.2021.100227
37. Bhattacharjee S, Macintyre CR, Wen X, Bahl P, Kumar U, Chughtai AA, Joshi R (2020) Nanoparticles incorporated graphene-based durable cotton fabrics. Carbon 166:148–163. https://doi.org/10.1016/j.carbon.2020.05.029
38. Karami Z, Youssefi M, Raeissi K, Zhiani M (2021) Effect of the morphology of silver layer on electrical conductivity and electrochemical performance of silver/reduced graphene oxide/cotton fabric composite as a flexible supercapacitor electrode. J Energy Storage 42:103042. https://doi.org/10.1016/j.est.2021.103042
39. Zhu L, Gao YY, Han B, Liu S, Fu XY, Ding H, Zhang YL (2019) Programmable laser patterning of Ag nanoparticles and reduced graphene oxide hybrid electrodes for nonenzymatic hydrogen peroxide detection. ACS Appl Nano Mater 2(12):7989–7996. https://doi.org/10.1021/acsanm.9b02032
40. Golsheikh AM, Huang NM, Lim HN, Zakaria R (2014) One-pot sonochemical synthesis of reduced graphene oxide uniformly decorated with ultrafine silver nanoparticles for non-enzymatic detection of H_2O_2 and optical detection of mercury ions. RSC Adv 4(69):36401–36411. https://doi.org/10.1039/C4RA05998K
41. Thangudu S, Kulkarni SS, Vankayala R, Chiang CS, Hwang KC (2020) Photosensitized reactive chlorine species-mediated therapeutic destruction of drug-resistant bacteria using plasmonic core–shell Ag@ AgCl nanocubes as an external nanomedicine. Nanoscale 12(24):2970–12984. https://doi.org/10.1039/D0NR01300E
42. Xue J, Li S, Lei D, Bi Q, Tang C, Xu N (2021) Multi-component Zn_2SnO_4/MoS_2/Ag/AgCl for enhancing solar-driven photoelectrocatalytic activity. Appl Surf Sci 544:148922. https://doi.org/10.1016/j.apsusc.2020.148922
43. Chambers BA, Afrooz AN, Bae S, Aich N, Katz L, Saleh NB, Kirisits MJ (2014) Effects of chloride and ionic strength on physical morphology, dissolution, and bacterial toxicity of silver nanoparticles. Environ Sci Technol 48(1):761–769. https://doi.org/10.1021/es403969x
44. Li G, Wang Y, Mao L (2014) Recent progress in highly efficient Ag-based visible-light photocatalysts. RSC Adv 4(96):53649–53661. https://doi.org/10.1039/C4RA08044K
45. Wang H, Zhang L, Chen Z, Hu J, Li S, Wang Z, Liu J, Wang X (2014) Semiconductor heterojunction photocatalysts: design, construction, and photocatalytic performances. Chem Soc Rev 43(15):5234–5244. https://doi.org/10.1039/C4CS00126E
46. You J, GuoY GR, Liu X (2019) A review of visible light-active photocatalysts for water disinfection: features and prospects. Chem Eng J 373:624–641. https://doi.org/10.1016/j.cej.2019.05.071
47. Xia MY, Xie Y, Yu CH, Chen GY, Li YH, Zhang T, Peng Q (2019) Graphene-based nanomaterials: the promising active agents for antibiotics-independent antibacterial applications. J Control Release 307:16–31. https://doi.org/10.1016/j.jconrel.2019.06.011
48. Xia D, An T, Li G, Wang W, Zhao H, Wong PK (2016) Synergistic photocatalytic inactivation mechanisms of bacteria by graphene sheets grafted plasmonic AgAgX (X = Cl, Br, I) composite photocatalyst under visible light irradiation. Water Res 99:149–161. https://doi.org/10.1016/j.watres.2016.04.055
49. Cheikhrouhou W, Ferraria AM (2020) Cotton fabrics decorated with nanostructured Ag/AgX (X: Cl, Br) as reusable solar light-mediated bactericides: a comparative study. Colloids Surf, B 196:111342. https://doi.org/10.1016/j.colsurfb.2020.111342

Publisher's Note Springer Nature remains neutral with regard to jurisdictional claims in published maps and institutional affiliations.

Springer Nature or its licensor holds exclusive rights to this article under a publishing agreement with the author(s) or other rightsholder(s); author self-archiving of the accepted manuscript version of this article is solely governed by the terms of such publishing agreement and applicable law.